

Simulation of radio plasma in clusters of galaxies

M.Brüggen^{1,2,3}, C.R.Kaiser⁴, E.Churazov^{1,5}, T.A.Enßlin¹

ABSTRACT

We present three-dimensional hydrodynamical simulations of buoyant gas in a typical cluster environment. The hot matter was injected continuously into a small region off-set from the cluster centre. In agreement with previous analytic estimates we found that the bubbles evolve very differently depending on their luminosity. Using tracer particles we computed radio maps of the bubbles based on different assumptions about the magnetic field. In the radio band the bubbles closely resemble FRI sources. For the bubbles to be detectable for long enough to account for FRI sources, we found that reacceleration has to take place. The bubbles are generally difficult to detect, both, in the radio and in the X-ray band. Thus it is possible to hide a significant amount of energy in the form of bubbles in clusters. Finally, we compute the efficiency of the bubbles to stir the ICM and find that recurrent low-power sources may be fairly effective in mixing the inner cluster region.

Subject headings: galaxies: active - galaxies: clusters: individual: Virgo - cooling flows - X-rays: galaxies

1. Introduction

The X-ray surface brightness of many clusters of galaxies shows a strong central peak which is generally interpreted as the signature of a cooling flow (Cowie & Binney 1977, Fabian & Nulsen 1977, Sarazin 1988, Fabian 1994). However, the simple cooling flow model conflicts with a growing number of observations that show that gas with a temperature below 1 keV is significantly less abundant than predicted. Searches for cold gas in the infrared and radio have detected far less mass than predicted. Therewhile, star formation can only account for a few percent of the predicted cooling rate.

Many clusters of galaxies host a radio source at

¹MPI für Astrophysik, Karl-Schwarzschild-Strasse 1, 85740 Garching, Germany

²International University Bremen, Campus Ring 1, 28759 Bremen, Germany

³Churchill College, Storey's Way, Cambridge CB3 0DS, UK

⁴Department of Physics & Astronomy, University of Southampton, University Road, Southampton SO17 1BJ, UK

⁵Space Research Institute (IKI), Profsovnaya 84/32, Moscow 117810, Russia

their centres. These radio sources emit large quantities of hot relativistic plasma into the intracluster medium (ICM). However, the problem of estimating the effect of the radio plasma on the ICM is substantially more intricate and difficult than the simple cooling flow model (Binney 2001). The radio source destroys the assumed spherical symmetry of the cooling flow. This makes the geometry more complex which is aggravated by the fact that magnetic fields with complex morphologies are likely to play an important role. Moreover, the radio source introduces dynamical motions into the medium pushing it out of hydrostatic equilibrium. To make matters worse, the source may even be time-dependent as many radio sources are believed to go through active and less active cycles. It is therefore difficult to come up with robust predictions. Nevertheless, the problem is important and, with the advent of more powerful X-ray telescopes, timely enough to explore it even with simplified models. Meanwhile, evidence for bubbles in the ICM is accumulating, especially from the X-ray telescope Chandra (Fabian et al. 2000, Mazzotta et al. 2001).

A hydrodynamic simulation of the full problem is currently beyond our possibilities as the scales involved vary enormously: The velocities range

from around 10 km/s in the outer cooling flow region to close to the speed of light in the radio jet. The densities and energy densities likewise vary by many orders of magnitude. Thus one may have to break the problem up into bits in order to make some progress.

Here we will focus on the later stages of the radio plasma, in which the bow shock of the initially overpressurised radio cocoon has vanished and the cocoon has come into approximate pressure equilibrium with its surroundings. The radio plasma then becomes Rayleigh-Taylor unstable and rises under the action of buoyancy forces to form plumes and mushroom-like structures (Churazov et al. 2001, Brüggén & Kaiser 2001). The displacement of thermal plasma by the relativistic plasma will suppress the X-ray emission and create “holes” such as observed in the Perseus cluster (Böhringer et al. 1993). Holes in the X-ray emission are also seen in the radio lobes of the Hydra A cluster (McNamara et al. 2000). On the other hand, the hot, buoyant radio plasma can entrain cooler ambient gas from the centre of the cooling flow and uplift it to the periphery thus enhancing the X-ray emission as observed in M87. Recently Saxton, Sutherland and Bicknell (2001) explained the radio and X-ray features of the middle lobe of Centaurus A on the basis of a buoyant bubble.

This little studied phase is the phase that we are considering in this paper. Thus this work differs from the work of Reynolds, Heinz and Begelman (2001) who simulated an earlier stage in the life of a radio cocoon, in which the cocoon expands supersonically and causes shocks in the cluster gas. This phase has also been studied numerically by Loken et al. (1993), Loken et al. (1995), Clarke, Harris & Carilli (1997), Balsara & Norman (1992), Tregillis, Jones & Ryu (2001) and Hardee & Clarke (1995). In the context of cooling flows jet simulations have been reported by Soker & Sarazin (1988), Soker (1997), Owen & Eilek (1998), Rizza et al. (2000), Sarazin, Baum, & O’Dea (1995), Zhao, Sumi, Burns, & Duric (1993) and Baum & O’Dea (1991). In this paper we will present 3D hydrodynamical simulations of buoyant gas in the ICM. We extend our previous work (Churazov et al. 2001, Brüggén & Kaiser 2001) by, first, going to three dimensions and second by considering a situation in which hot gas is *continuously* injected into a small region close to the centre of the grav-

itational potential.

The idea that buoyancy plays an important role in the evolution of the radio lobes in galaxies has been first proposed by Gull and Northover (1973) and has been used to estimate the life time of the radio lobes in M87 by Böhringer et al. (1995). Three-dimensional simulations of hot bubbles in a stratified stmosphere have also been presented by Brandenburg & Hazlehurst (2001).

For the simulations presented below a particularly relevant observational example is perhaps Hydra A – a radio galaxy associated with a relatively poor cluster A780. In the radio Hydra A (3C 218) is a powerful Fanaroff-Riley type I source with extended double radio lobes (e.g. Ekers & Simkin 1983, Taylor et al. 1990), suggesting continuous activity of the central engine for long period of time. Recent Chandra observations (McNamara et al., 2000, David et al., 2001) clearly demonstrated the interaction between the radio emitting plasma and the thermal gas. The morphology of the interacting region is somewhat different from that observed in M87. In Hydra A thermal gas has clearly been pushed out of those regions that contain the radio plumes.

2. Method

2.1. Hydrodynamical simulations

The simulations were obtained using the parallel version of the ZEUS-3D code which was developed especially for problems in astrophysical hydrodynamics (Clarke & Norman 1994). The code uses finite differencing on an Eulerian grid and is fully explicit in time. It is based on an operator-split scheme with piecewise linear functions for the fundamental variables. The fluid is advected through a mesh using the upwind, monotonic interpolation scheme of van Leer. For a detailed description of the algorithms and their numerical implementation see Stone & Norman (1992a, b). In order to study the spectral ageing of the relativistic gas, the ZEUS code was modified to follow the motion of ‘tracer’ particles which are advected with the fluid.

In our simulations we employed an ideal gas equation of state and we ignored the effects of magnetic fields and rotation. The cooling time is sufficiently long compared to the time scales



Fig. 1.— Initial distribution of electron density, temperature, pressure and gravitating mass (adopted from Nulsen and Böhringer 1995) assumed in the simulations.

considered here since, for an electron density of 0.02 cm^{-3} and temperature of the order of 2 keV (see Fig.1) the cooling time is $\sim 5 \times 10^8$ years. This is one order of magnitude longer than the typical duration of the run of $\sim 5 \times 10^7$ years. We therefore completely neglected cooling. The simulations were computed on a Cartesian grid in three dimensions. The serial version of the code was run on SUN ULTRA workstations and the parallel version on an SGI ORIGIN 3000. The computational domain spanned 30 kpc in height with a base area of $10 \text{ kpc} \times 10 \text{ kpc}$. This domain was covered by $450 \times 150 \times 150$ grid points. On all boundaries the boundary conditions were chosen to be outflow conditions.

The initial mass and temperature distributions were modelled on the Virgo Cluster as given by Nulsen & Böhringer (1995) (see Fig.1). The gas density distribution was then found by assuming hydrostatic equilibrium to maintain an initially static model. The pressure scale height varied from around 1 kpc near the centre to around 40 kpc at the edge of the simulated region. At each

timestep gas was injected into a spherical region with a radius of $r_b = 0.7 \text{ kpc}$ at a distance of $d = 9 \text{ kpc}$ from the gravitational center. This injected gas was in pressure equilibrium with its surroundings. It was hotter than the ambient gas by a factor of 100-400 and had zero initial velocity. At the start of the simulation 24000 tracer particles were uniformly distributed throughout the computational domain. Subsequently, at certain intervals new, uniformly distributed tracer particles were added into the spherical injection region. The gas was treated as a single fluid and was assumed to obey a polytropic equation of state with $\gamma = 5/3$. As we discuss in detail below, buoyancy drives the hot gas through the ambient medium as shown in Fig.2.

Finally, we should address some issues related to the accuracy of these kinds of finite-difference hydrodynamical simulations. First, one can note that the density in the bubble increases. While the code can simulate large-scale mixing due to Rayleigh-Taylor and Kelvin-Helmholtz instabilities, it does not include real diffusion of particles. Any observed diffusion is therefore entirely numerical. The boundary between the bubble and the ambient medium also becomes less sharp as the simulation proceeds due to discretization errors in the advection scheme. For a test of the advection algorithm in the ZEUS code see Stone & Norman (1992). In simple advection tests it was found that during the advection of a sharp discontinuity over a grid of 200 zones the discontinuity is spread over 3-4 grid cells. Therefore, the small features in our simulation are likely to be affected by these advection errors whereas the larger features are not.

Second, numerical viscosity is also responsible for suppressing small-scale instabilities at the interface between the bubble and the cooler, surrounding, X-ray emitting gas. To assess the effects of numerical viscosity, we have repeated our simulations on grids with lower resolution. From our experiments we can conclude that 'global parameters' such as the position and size of the 'mushrooms' as well as the presence of "toroidal" structure are relatively insensitive to the resolution. The detailed developments of the morphology on small scales do depend on the resolution and the initial conditions.

2.2. Simulation of the radio emission

Radio synchrotron emission arises from relativistic, magnetised plasma. The simulations presented in this paper are based on a purely hydrodynamical scheme with a single, non-relativistic fluid. To obtain radio maps of the simulations we have to make a number of simplifying assumptions which we summarise briefly below. These and the method by which we calculate the synchrotron surface brightness of the simulated flow are described in greater detail in Churazov et al. (2001).

- The magnetic field is tangled on scales that are much smaller than the scales of fluid motions. Therefore, the relativistic plasma consisting of magnetic fields and relativistic particles is confined to small ‘bubbles’ intermixed with the non-relativistic, thermal plasma. The size of these bubbles will in practice be set by the tangling scale of the magnetic fields. Thus the two fluids are separated on microscopic scales.
- The bubbles of relativistic plasma are in pressure equilibrium with the surrounding thermal gas. We further assume that they expand and contract adiabatically with an adiabatic index of $4/3$. For consistency the volume filling factor of the relativistic plasma must be small so that its influence on the total fluid flow is negligible.
- The pressure of the relativistic plasma is given by the sum of the energy density of the magnetic field, u_{mag} , and that of the relativistic particles, u_{rel} . As this is balanced at all times by the thermal pressure, p_{th} , we have $3p_{\text{th}} = u_{\text{mag}} + u_{\text{rel}}$. This sets the initial conditions for the relativistic plasma at the time when it is injected into the computational grid together with the thermal gas. In the following we investigate two cases: Either the magnetic field is uniform throughout the injection region with a value corresponding to the equivalent magnetic field of the Cosmic Microwave Background (CMB), i.e. $B = \sqrt{8\pi u_{\text{CMB}}} = 3.18(1+z)^2 \mu\text{G}$ (where z is the cosmological redshift; e.g. Leahy 1991) and so $u_{\text{rel}} = 3p_{\text{th}} - u_{\text{CMB}}$, or we assume equipartition between the magnetic field and the relativistic particles, i.e.

$$u_{\text{mag}} = u_{\text{rel}} = 3/2 p_{\text{th}}.$$

- We assume that the relativistic particles are injected into the flow with a power law energy distribution, i.e. $n_e d\gamma = n_0 \gamma^{-p} d\gamma$ where γ is the Lorentz factor of the particles. We set $p = 2$ and impose cut-offs so that $1 \leq \gamma \leq 10^6$. The normalisation of the particle spectrum, n_0 , is determined by the value of u_{rel} .

The exact synchrotron spectrum also depends on the energy distribution of the emitting relativistic electrons. This in turn is determined by the form of injection of these particles into the flow and subsequent energy losses due to adiabatic expansion, synchrotron radiation and inverse Compton scattering of the CMB. To determine the energy distribution at a given place and time, we use the tracer particles that are continuously injected with the gas into the flow. These tracer particles are advected with the fluid and their ‘pressure history’ is frequently recorded in the course of the simulation. This completely determines the energy distribution of the relativistic particles at their respective positions within the flow. Details of the method can be found in Churazov et al. (2001). Making assumptions about the strength of the magnetic field, the local synchrotron emissivity can be calculated from the energy distribution of the relativistic particles. The radio surface brightness is then determined by integration along lines of sight through the computational domain.

We assume that the material in the injection region of our simulations is supplied by the jet of an Active Galactic Nucleus (AGN). The flow in the jet from the centre of the source to the injection region is taken to be ballistic. This implies that the pressure within the jet declines very rapidly along the flow thus making the jet underpressured with respect to its environment. The injection region may then be identified with the location of a strong internal shock which brings the jet into pressure equilibrium with the surrounding gas (e.g. Cantó & Raga 1991) thus making the jet susceptible to turbulent disruption. This simplified interpretation is also motivated by the observations of radio galaxies of type FRI (Fanaroff & Riley 1974). They often show well-collimated, apparently lam-

inar jets in the inner regions which start to flare into wider, more turbulent structures further out (e.g. Muxlow & Garrington 1991). In most of our simulations material is injected with zero initial velocity. This would imply that all bulk kinetic energy is dissipated by the shock at the location of the injection region.

3. Results and discussion

3.1. Morphology of the plumes

In Fig. 2 and 3 we show snapshots of the density and specific entropy distribution in a vertical slice through the computational domain. In this run the luminosity of the injected gas was 4.4×10^{41} erg s⁻¹ (subsequently called run 1).

One can note that the hot gas can travel to large heights before it is slowed down by the excess pressure that has built up at the bow of the plume. The gas is then driven sideways to form a mushroom-like structure. The plume is also not cylindrically symmetric but meanders a bit like the smoke from a candle and breaks up into a number of irregular fragments.

The plume or 'nozzle' of hot gas is disrupted by Kelvin-Helmholtz instabilities as discussed, e.g., by Smith et al. (1983). The shear between the rising hot fluid and the ambient medium creates a vortex boundary layer that destroys the upward flow and mixes the fluid into the ambient medium. In particular, shear causes the formation of tori which separate from the main plume. This process, also called "vortex shedding", has been observed and studied extensively (see Norman et al. 1982). As a rule of thumb one can say that if the plume is thinner than a scale height of the ambient medium, the jet breaks up into a turbulent wake of bubbles. Smith et al. (1983) have worked out a minimum luminosity for a jet to maintain an uninterrupted flow. For a sound speed ratio between the ICM and the bubble of $c_b/c_{\text{ICM}} \sim 10$ as in our simulations, the minimum luminosity is of the order of $L_{\text{min}} \sim L_c c_{\text{ICM}}/c_b$, where $L_c = p_{\text{ICM}} c_{\text{ICM}} h^2$ with h being a pressure scale height of the ICM, and p_{ICM} the pressure. (All values are taken at the location of the bubble.) In our case $h \sim 10$ kpc, $c_{\text{ICM}} \sim 4 \times 10^7$ cm s⁻¹ and $p_{\text{ICM}} \sim 10^{-10}$ erg cm⁻³ giving $L_{\text{min}} \sim 3.5 \times 10^{41}$ erg s⁻¹. So the luminosity in

our simulation is near this analytical estimate for the minimum luminosity for a steady jet.

One should also note that the results of the 3D simulations are different from the results of two-dimensional simulations in which the boundary coincides with the axis of symmetry. They usually show strong flows along the boundary (sometimes called "axis jets") and do not reproduce the correct rise velocities.

It is easily shown that the order of magnitude of the terminal velocity of the gas is

$$v \sim \sqrt{g \frac{V}{S} \frac{2}{C} \frac{\rho_a - \rho_b}{\rho_a}} \sim \sqrt{g \frac{V}{S} \frac{2}{C}} \quad (1)$$

where V is the bubble volume, S is the cross section of the bubble, g is the gravitational acceleration (we assume the ambient gas is in the hydrostatic equilibrium), ρ_a and ρ_b are the mass densities of the ambient and the bubble gas densities respectively. The numerical coefficient C (drag coefficient) depends on the geometry of the bubble and the Reynolds number. For a solid sphere moving through an incompressible fluid the drag coefficient C is of the order 0.4–0.5 for Reynolds numbers in the range $\sim 10^3$ – 10^5 . Here the factor of $(\rho_a - \rho_b)/\rho_a$ can be dropped if the bubble density is low compared to the ambient gas density. The expression for the terminal velocity can be rewritten further using the Keplerian velocity at a given distance from the cluster center: $v \sim \sqrt{(r/R)(8/3C)} v_K$, where r is the bubble radius, R is the distance from the center and $v_K = \sqrt{gR}$ is the Keplerian velocity. In our simulations, the typical Keplerian velocity was ~ 400 km/s. Even though this is just an order of magnitude estimate of the rise velocity it is approximately correct since the velocity depends only weakly (as the 0.5 power) on the bubble size and gas density gradients.

In a second simulation the energy is injected into a region of radius $r = 1$ kpc with a luminosity of 3.8×10^{42} erg s⁻¹ (subsequently called run 2). The evolution of the density in this run is shown in Fig. 6. Now a much broader plume rises that is not disrupted and a steady jet forms. Only later secondary Rayleigh-Taylor instabilities set in that

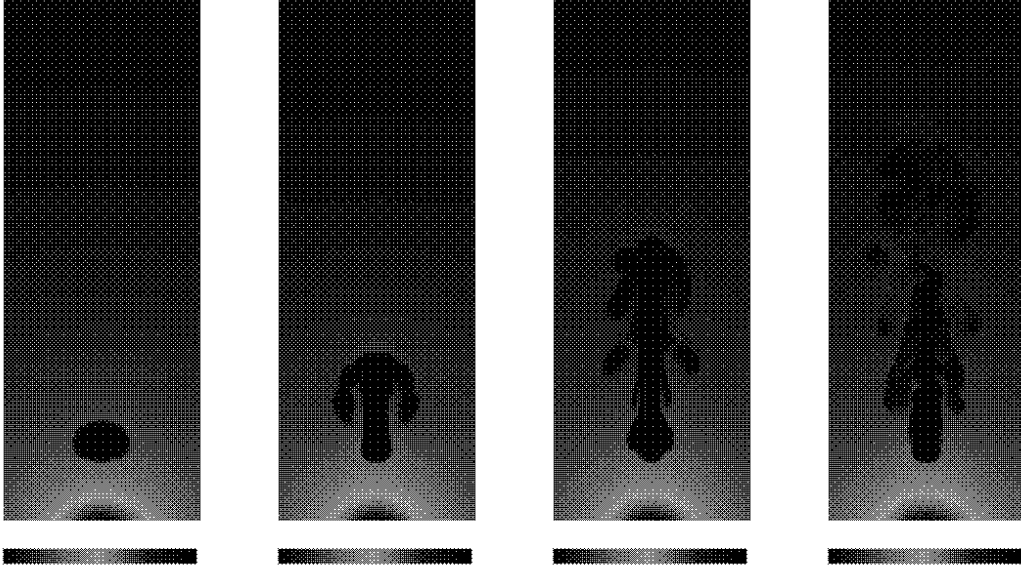


Fig. 2.— Snapshots of density at in a vertical slice through the computational domain for $L = 4.4 \times 10^{41}$ erg s $^{-1}$ at times 8.36, 25, 41 and 58.5 Myrs.

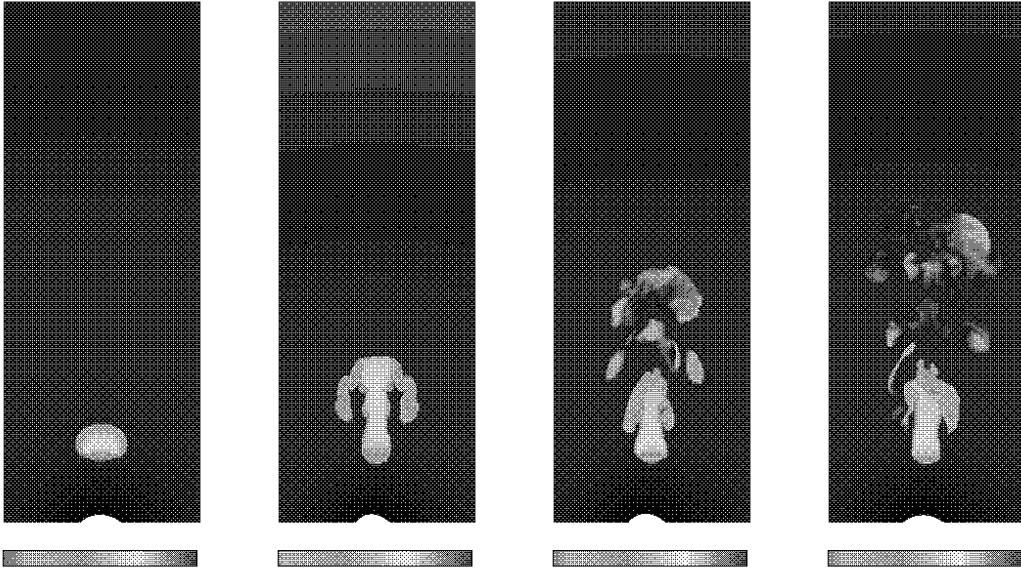


Fig. 3.— Snapshots of specific entropy in a vertical slice through the computational domain for $L = 4.4 \times 10^{41}$ erg s $^{-1}$ at the same times as in the previous plot.

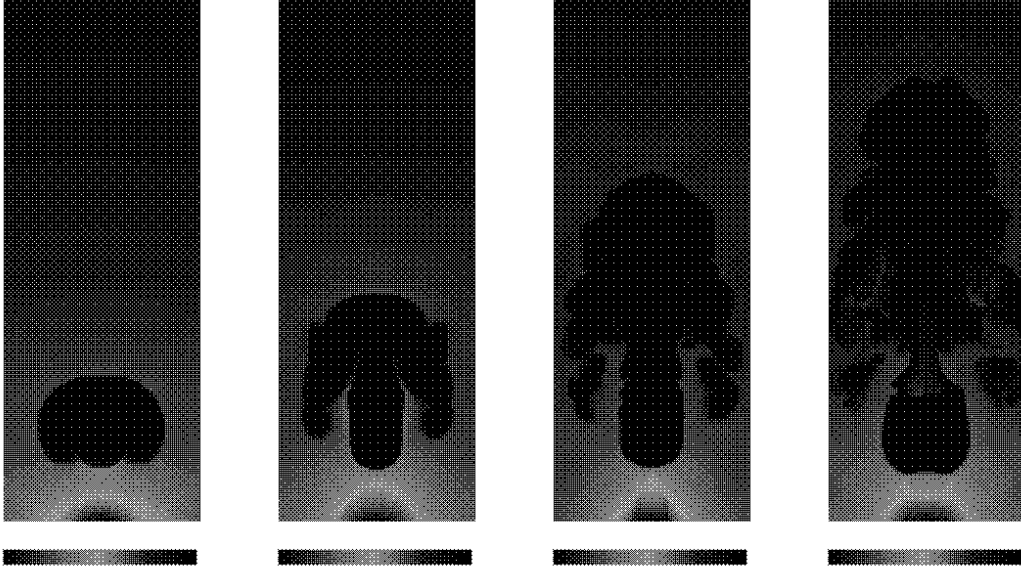


Fig. 4.— Snapshots of the density in a vertical slice through the computational domain for $L = 3.8 \times 10^{42}$ erg s $^{-1}$ at times 12.5, 25, 37.6 and 50 Myrs.

form turbulent mushroom structures.

In this paper we will focus on the two runs described above (run 1 and 2). However, in order to probe the parameter ranges for which our study applies, we have made two further simulations, in which the dynamics of the flow turned out to be very different.

In Fig. 5 we show the density for a run with an even higher luminosity of 10^{44} erg s $^{-1}$ (run 3). In this simulation the computational domain span 20 kpc in height with a base area of 16 kpc \times 16 kpc. Now the bubble evolves very differently. A huge bubble is blown up before it can rise and split into smaller fractions. This behaviour is described by Smith et al. (1983) who estimate that for luminosities $L > 6 L_{\text{min}}$ the injected matter forms bulky clouds rather than narrow jets. The flow no longer has the form of a nozzle and is not in equilibrium. The pressure gradient perpendicular to the symmetry axis cannot confine the jet and recurrent nozzle choking takes place. These are order-of-magnitude estimates and we find that the maximum luminosity is higher than the above estimate by a factor of a few. But our simulations are in rough agreement with the behaviour predicted by these simple analytical estimates.

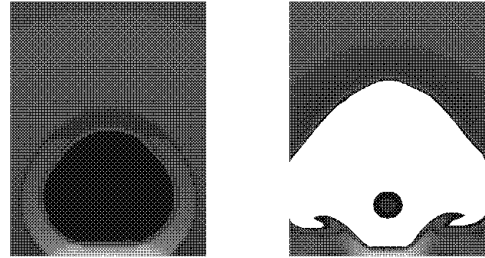


Fig. 5.— Snapshots of the density in a vertical slice through the computational domain for $L = 10^{44}$ erg s $^{-1}$ after 5 and 10 Myrs.

Finally we performed a simulation where the injected material was given an initial velocity pointing radially outward (run 4). The velocity was chosen to be three times the sound speed of the local ambient medium. Thus the kinetic energy of the injected gas was still many orders of magnitude smaller than the thermal energy. It is apparent that the jet now evolves on a much shorter time scale. The flow is much more laminar than in the purely buoyant case and not governed by Rayleigh-Taylor instabilities. The jet terminates at a shock that is driven outward with a velocity that is close to the injection velocity. One can note that the evolution is quite different in the cases with and without an initial velocity. This is discussed in more detail in the next section.

The rising bubbles stir convective motions in the cluster atmosphere and therefore may help to erase the temperature gradient by turbulent mixing. In order to measure this effect we trace individual fluid elements in the cluster atmosphere using tracer particles and calculate the statistics of their displacements. The particles are binned according to their initial cluster radius r_0 and then the mean displacement in radial direction $\delta r(r_0, t) = \langle r(r_0, t) - r_0 \rangle$ and its dispersion $\sigma_r(r_0, t) = \langle (r(r_0, t) - r_0)^2 \rangle^{1/2}$ are computed. The brackets $\langle \dots \rangle$ denote the average over all tracer particles within a spherical half-shell, including virtual particles outside the simulation volume, which were assumed to be at rest. Furthermore, the quantities $\delta l(r_0, t) = \langle |\vec{r}(\vec{r}_0, t) - \vec{r}_0| \rangle$ and $\sigma_l(r_0, t) = \langle |\vec{r}(\vec{r}_{\text{initial}}, t) - \vec{r}_0|^2 \rangle^{1/2}$ were calculated. The profiles of these quantities at the end of the simulation are shown in Figs. 7 and 8, and their temporal evolution at several initial cluster radii in Fig. 9.

The relative heights of the profiles in Fig. 7 indicate that there is only a small net displacement of the tracer particles compared to their dispersion, and that both the dispersion and the net displacement are predominantly in the vertical direction. One can see that the dispersion decreases with radius. This is partly because the estimated volume averages are calculated for spherical shells, whose volume increases as r^2 , whereas the simulated jet only affects a finite and roughly constant area perpendicular to the jet axis.

The temporal evolution of the tracer particle dispersion in radial direction as shown in Fig. 9

shows a time-lag, owing to the time the radio plasma needs to ascend. Then one can note a small bump due to the uplifting of gas by the passing bubble. This is followed by a linear growth of σ_r . This linear time-dependence indicates that the regime of turbulent diffusion, in which $\sigma_r \propto t^{1/2}$, is not yet reached. However, the flow pattern imprinted by the rising bubbles is able to transport gas to larger radii. The average radial displacement of the gas within the whole 30 kpc half-sphere is $\bar{\sigma}_r = 0.44$ kpc after 75 Myr, and $\bar{\sigma}_r = 0.91$ kpc after 125 Myr at the end of the run 1. At the end of run 2, after 75 Myr, the average displacement is $\bar{\sigma}_r = 1.38$ kpc. Since the jet power differed by about one order of magnitude in the two runs, the mean square displacement of the environment $\bar{\sigma}^2$ is proportional to the jet power. Hence the mean displacement varies like the square root of the power. As the latter is the crucial quantity describing the mixing efficiency, this suggests that, over a longer period, frequent low-power activity cycles are more efficient in stirring the environment than less frequent high-power outbursts of comparable energy output. We hope that this can be confirmed in future simulations.

We have also plotted the evolution of the particles for run 4, where the radio plasma was given an initial velocity (see Fig. 9). It is apparent that the efficiency to uplift and mix gas increases significantly when the plasma carries a small amount of initial kinetic energy.

3.2. Synchrotron emission from the flow

Our interpretation of the injection region is that this is the site of a strong shock caused by a jet emanating from an AGN. This shock may accelerate electrons and, depending on the composition of the jet, positrons to relativistic energies. If the jet carries a magnetic field, we expect to observe radio synchrotron emission from the injected gas. Using the assumptions and method summarised in Section 2.2 we calculated the surface brightness due to synchrotron radiation from our simulations. In order to make the results directly comparable to our earlier simulations of M87 (Churazov et al. 2001), we assumed an observing frequency of 327 MHz and a distance of 18 Mpc, appropriate for the Virgo cluster. Here we assume a volume fill-

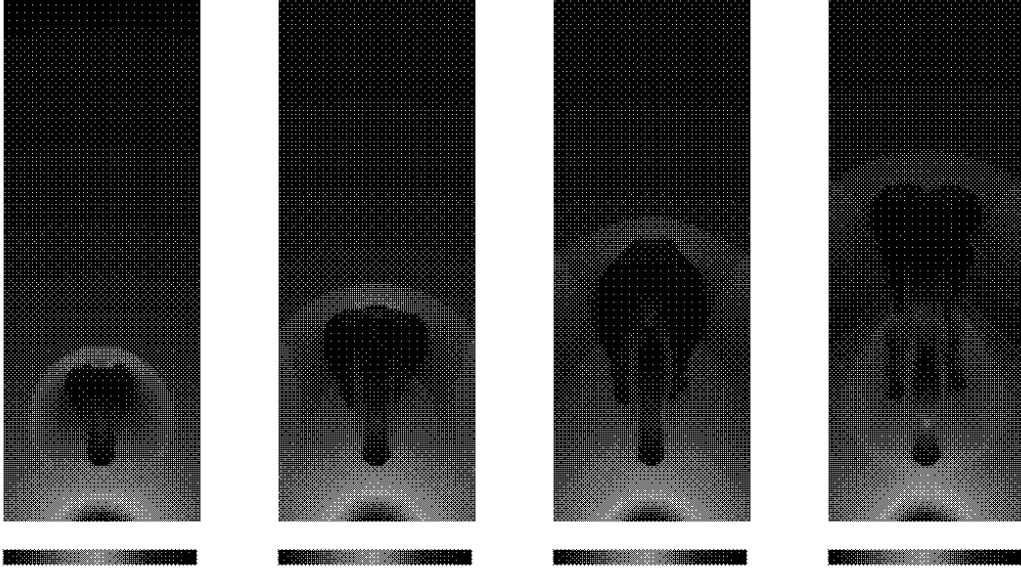


Fig. 6.— Snapshots of the density in a vertical slice through the computational domain for a simulation with an initial velocity of $2.8 \times 10^8 \text{ cm s}^{-1}$ and $L = 4.4 \times 10^{41} \text{ erg s}^{-1}$ at times 3.8, 7.5, 11.2 and 15.1 Myrs.

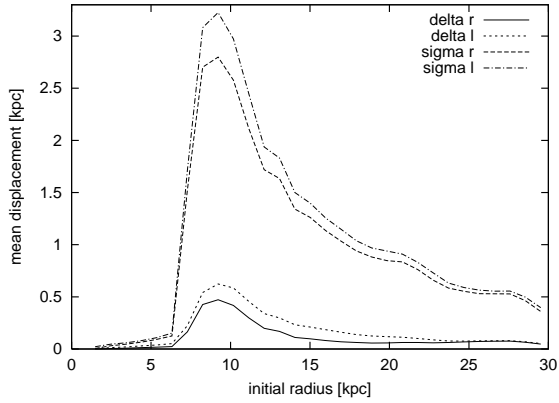


Fig. 7.— Radial profiles of the average particle displacement at the end of the simulation time as a function of the initial cluster radius for run 1. For details and discussion see the text.

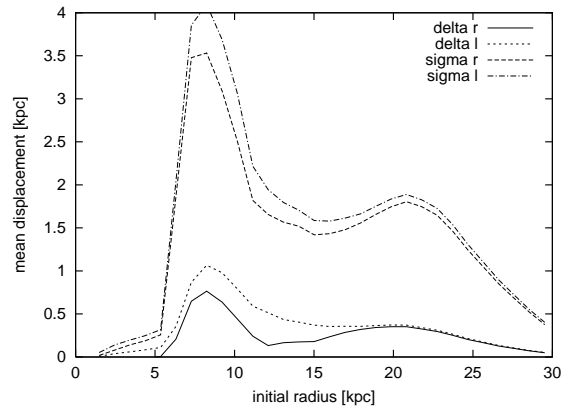


Fig. 8.— Radial profiles of the average particle displacement at the end of the simulation time as a function of the initial cluster radius for run 2.

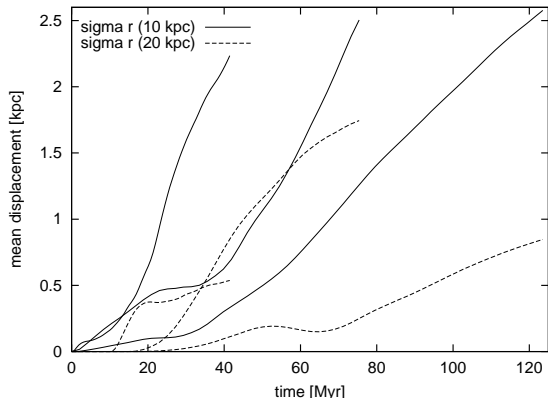


Fig. 9.— Temporal evolution of the average radial dispersion of tracer particles for different initial cluster radii. The lines that terminate at 41 Myrs correspond to run 4, those that terminate at 75 Myrs correspond to run 2, the other ones to run 1. For details and discussion see the text.

ing factor of unity for the radio plasma even if we require implicitly a lower volume filling factor for the plasma to have a negligible influence on the dynamics. The results can easily be scaled for lower filling factors.

Figure 10 shows the results for the radio surface brightness for our simulation with low luminosity (run 1). In the upper row the strength of the magnetic field corresponds to the equivalent field of the CMB. This implies that the field and the relativistic particles are far from equipartition. The energy stored in the magnetic field exceeds that in the particles by a factor of several hundred. Therefore, the plasma is not very efficient in emitting synchrotron radiation but the lifetime of the relativistic particles is maximised (e.g. Churazov et al. 2000). For this case, the radio surface brightness is a good tracer of the pressure distribution within the flow as in our approach the strength of the magnetic field is coupled to the thermal pressure. In the last panel ‘holes’ in the radio structure due to cumulative radiative and expansion losses of the relativistic particles are clearly visible. Despite these, the radio structure closely follows the flow structure. In the early stages the brightest parts of the flow are in the injection region and at the leading edge of the rising bubble. The former is caused by the presence of freshly accelerated relativistic particles in a region of compar-

atively high pressure. The latter shows the action of the ram pressure of the external gas being pushed aside in compressing the buoyant bubble. Fluid instabilities cause the flow to develop turbulent structures at later times and these are traced by the radio emission. Local pressure enhancements caused by the turbulent motion are visible as slightly brighter filaments in the radio maps.

In the lower row of Figure 10 we show the results for the same simulation but now we assume initial equipartition between the energy in the magnetic field and the energy of the relativistic particles. This is close to the energy distribution which is most efficient in producing the synchrotron radiation (e.g. Longair 1994). Again the injection region is the most prominent feature in the radio maps. However, radiative energy losses are now much more severe. Thus even in the early stages of the simulation significant parts of the buoyant flow are not observable in the radio. Only until about 40 Myrs into the simulation can the ram-pressure compressed leading edge of the bubble be recognised in synchrotron emission. At this time it has reached a height of roughly 19 kpc. At later times the energy losses of the relativistic particles are too strong and we only see the lower parts of the ‘chimney’ excavated by the buoyant material. However, the twisting of the flow in the chimney induced by fluid instabilities is clearly visible. The radio emission gives the impression of a candle flame under the influence of some air draft passing by.

3.3. Comparison with observations of radio galaxies

The radio maps in the upper row of Figure 10 resemble the morphology of radio galaxies of type FRI. The gas flow is relatively laminar after leaving the injection region but becomes increasingly turbulent in the outer regions. However, there are a number of problems with a direct comparison of the simulations with observations of FRI objects. Firstly, our simulations assume a vanishing initial flow velocity in the injection region. This is certainly not the case in FRI objects where the flow velocities even after the jet flaring are at least mildly relativistic. All outward motion in our simulations is induced by buoyancy of the hot gas in the injection region. It is therefore not surprising that the rise of the turbulent flow region

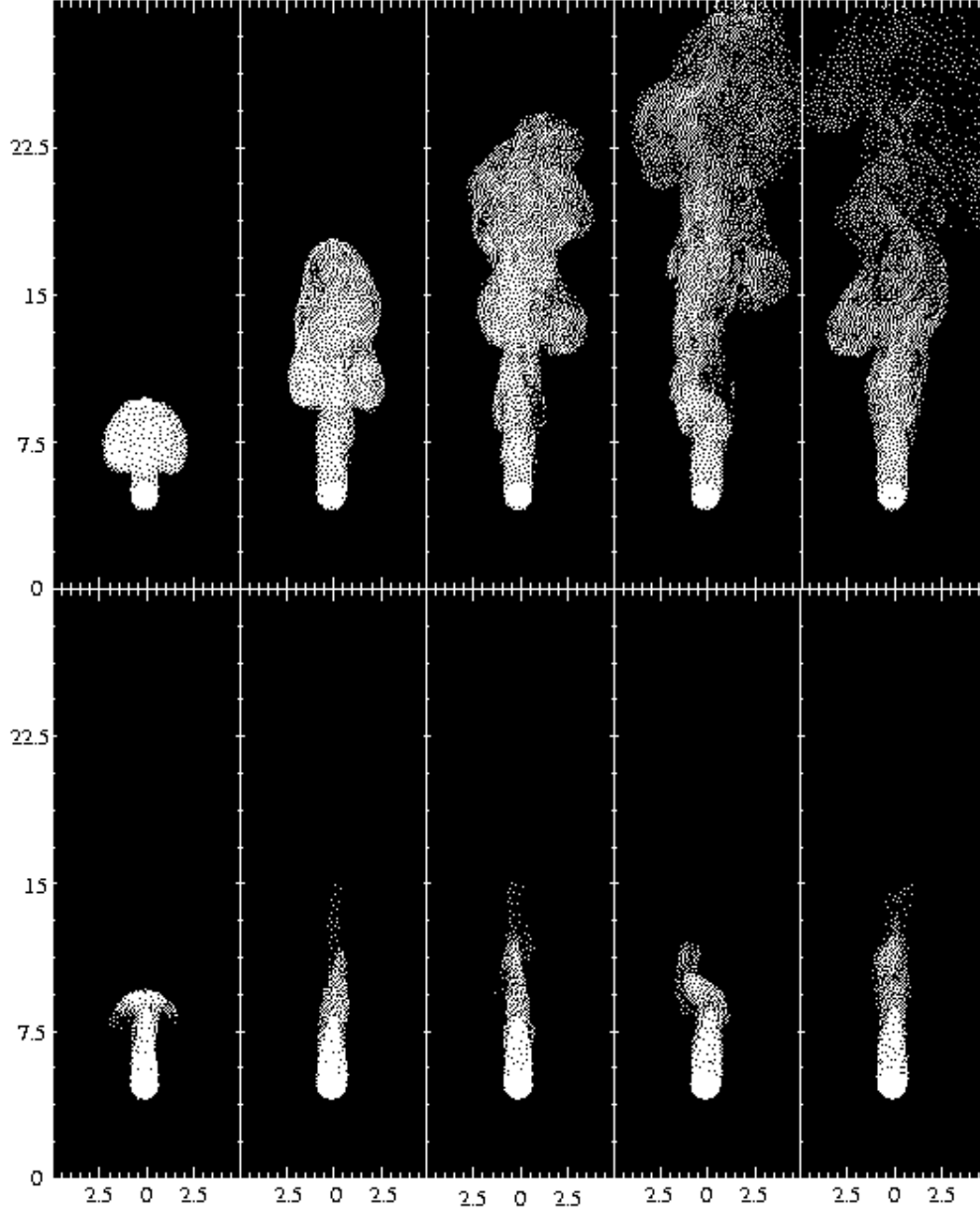


Fig. 10.— Radio surface brightness at times (from left to right) 23.1, 44.1, 65.1, 86.1 and 107.1 Myrs after the start of the simulation (run 1). The axes are labelled in units of kpc. Individual pixels have a size of $0.1 \times 0.1 \text{ kpc}^2$ which corresponds to $1.15 \times 1.15 \text{ arcsec}^2$ at the assumed distance of 18 kpc. Upper row: The magnetic field is initially set to the equivalent field of the CMB. Filled contours are logarithmic in steps of 2 starting from $20 \mu\text{Jy}$ per pixel (black) to 10.2 mJy (white). Lower row: The energy density of the magnetic field is in equipartition with that of the relativistic particles. Filled contours are logarithmic in steps of 2 starting from $200 \mu\text{Jy}$ per pixel (black) to 102 mJy (white).

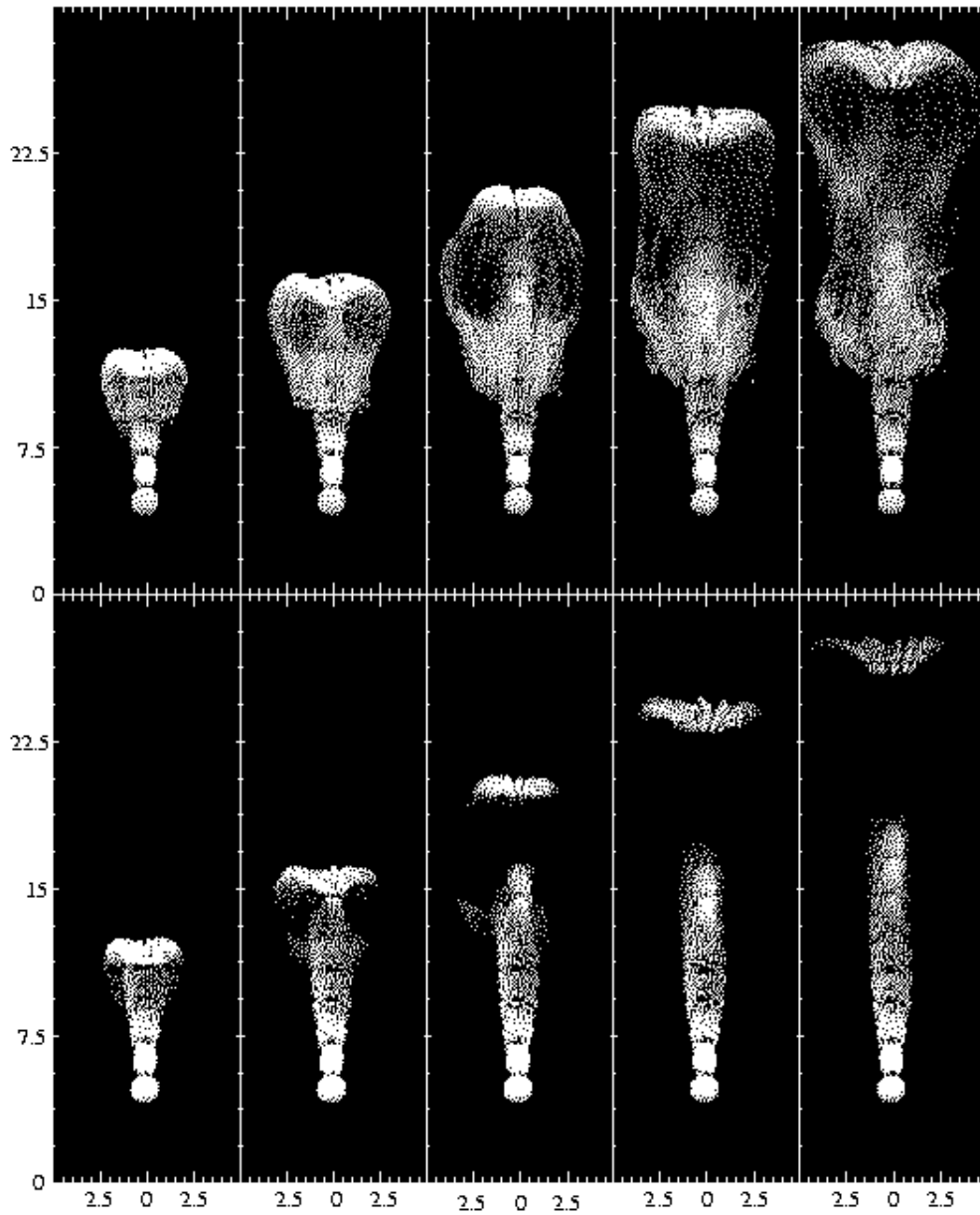


Fig. 11.— Radio surface brightness maps for the low-resolution simulation with non-zero initial velocity of the injected gas (see text). Contours and labels as in Figure 10. Simulation time of panels from left to right: 6.3, 11.3, 16.4, 21.4 and 26.5 Myrs.

out to tens of kiloparsecs proceeds on timescales exceeding the lifetime of the relativistic electrons responsible for the synchrotron emission. Unless there is significant re-acceleration of relativistic particles in the turbulent part of the flow, models with purely buoyant motion will not be able to explain observations of FRI objects spanning more than 1 Mpc (e.g. 3C 31, Leahy, DRAGN Atlas⁶). Moreover, the energy injection rates in our simulations are much smaller than the typical energies of radio jets of about $5 \times 10^{44} \text{ erg s}^{-1}$ (Owen, Eilek & Kassi 2000). However, what these simulations tell us, is that it is possible to inject a considerable amount of energy into clusters without producing strong observational signatures. It is thus possible that a significant amount of energy may be hidden in clusters which is not easy to detect (also see Enßlin 1999).

To investigate the effect of a non-zero initial velocity we performed a simulation in which the material in the injection region is given an initial velocity that points radially outward (upward in all Figures presented in this paper). Figure 11 shows the synchrotron radio maps for this simulation (run 4). The brightest feature is the strong compression in the flow just above the injection region. There is a secondary, weaker compression within the developing laminar flow that moves outwards and produces another enhancement of the surface brightness. From theoretical arguments it is well known that the radius of a collimated, laminar gas flow oscillates about its equilibrium radius, i.e. the radius which would allow the flow to be in pressure equilibrium with its surroundings (e.g. Bridle, Chan & Henriksen 1981). The flow expands and accelerates until it is underpressured with respect to its surroundings. A compression and deceleration region will follow resulting in the pressure inside the flow to rise above that of the ambient medium. This behaviour can recur many times. In our simulations it leads to the formation of bright ‘knots’ within the laminar gas flow. In supersonic flows this expansion and re-collimation often leads to the formation of shocks (e.g. Wilson & Falle 1985). Although the injected material in our simulation reaches Mach numbers of up to 5 in the acceleration regions, the re-collimation cur-

vature radius is so small that the flow does not develop a shock (Icke 1991).

The leading edge of the rising bubble proceeds at a much higher speed than in the purely buoyant case. The rise of the flow ends in a shock which is clearly visible due to the strong compression of the gas it causes. Unlike in the purely buoyant case, the growth time of the fluid instabilities is now too long to significantly disrupt the laminar flow from the injection region. At later times the gas flow is increasingly protected by the developing lobe of material flowing back from the region where the rising gas impacts on the surrounding medium. These features, a shock at the end of the laminar flow and the lobe inflated around the rising flow, are well-known features of radio galaxies of type FRII. They have been studied in great detail in numerous numerical simulations. However, it is interesting to note that the transition from turbulent flow to a self-protecting and self-collimating laminar one occurs quite abruptly when adding an initial velocity to the injected gas. Since the gas in the jets of FRI-type radio galaxies is known to have high velocities, they most probably become turbulent solely through the destabilizing entrainment of gas from their surroundings.

3.4. The rising bubble in X-ray emission

In Fig.12 we have plotted the X-ray surface brightness associated with our simulation 1 and 2. The surface brightness was calculated by integrating the emissivity along the line of sight. The density and the temperature outside the computational volume were assumed to take their undisturbed values. Red/blue colour correspond to regions where the X-ray surface brightness is 20-25 % brighter/dimmer than the undisturbed brightness. Green colour indicates that the surface brightness is close to the undisturbed value. One can note that the effect of the hot plasma on the X-ray surface brightness is relatively small. The luminosities that we have considered here are 1 - 2 magnitudes smaller than that of a typical radio jet or the X-ray luminosity. Thus, we can conclude that radio plasma injected with luminosities $\sim 10^{42} \text{ erg s}^{-1}$ is not easy to detect in X-ray observations.

⁶Available at <http://www.jb.man.ac.uk/atlas/>

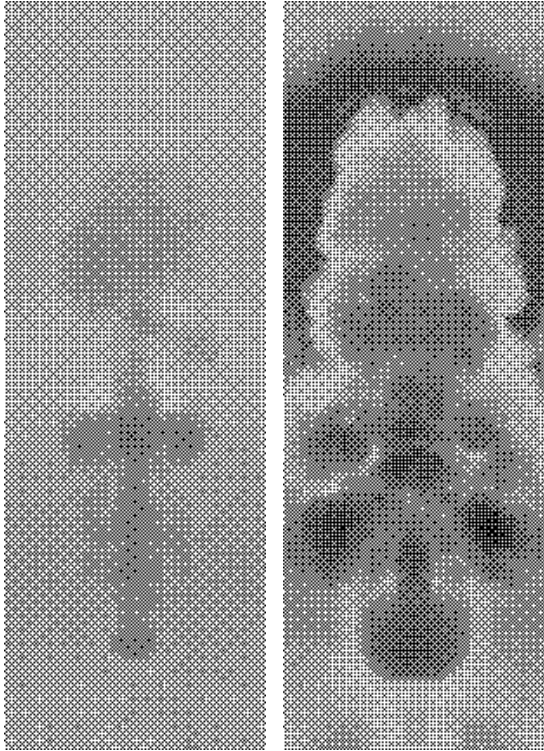


Fig. 12.— X-ray surface brightness relative to the undisturbed cluster for run 1 (left) and run 2 (right).

4. Conclusions

In this paper we presented high-resolution 3D simulations of buoyant bubbles in a typical cluster environment. The aim was to compute the appearance of these buoyant bubbles in radio and x-ray observations, and to study the impact of the bubbles on the ICM. Depending on the luminosity of the injection region, we found a qualitatively different behaviour of the fluid flow. For low luminosities of around 10^{41} erg s^{-1} the thin stream of hot gas breaks up into a series of rising bubbles. For higher luminosities a broad, steady stream develops that forms a mushroom-like structure via Rayleigh-Taylor instabilities. For luminosities greater than $\sim 10^{43}$ erg s^{-1} huge cavities are blown up before they can rise through the medium. These findings are in rough agreements with estimates by Smith et al. (1983).

We produced radio maps of the rising bubbles assuming that relativistic particles and magnetic fields are injected alongside the thermal gas in the injection region. Following the energy loss history of these particles, we could calculate the radio emission. For very low magnetic fields (comparable to the equivalent field of the CMB) we find that the radio emission closely traces the pressure distribution within the flow. Filaments of enhanced radio emission can be identified as turbulent compression regions. For equipartition, the life time of the relativistic particles is significantly shorter than the flow timescale and only those parts of the flow close to the injection region are detectable.

The morphology of the radio emission resulting from our simulations is reminiscent of FRI-type radio galaxies. However, all fluid motion is induced by buoyancy alone and the involved timescales are thus so long that it is unlikely that any such source would be detectable in the radio. If the gas is injected with a non-zero outward velocity, then the flow timescale reduces greatly and may become shorter than the lifetime of the relativistic particles. However, in this case the flow shows the typical self-collimation through alternating expansion and contraction zones. The morphology of such a flow is more similar to that of FR II-type radio galaxies.

In this paper we have not addressed the possibility of re-acceleration of relativistic particles within the turbulent flow. This effect may make the flow detectable in the radio even after the initially accelerated relativistic particles would have faded. However, these processes are not well understood and we therefore do not attempt to include them here.

In addition to the radio maps, we produced maps of the X-ray surface brightness. Similar to the radio maps, we found that our bubbles do not leave a strong signature in the surface brightness. What this tells us is that it is possible to hide a lot of energy in form of buoyant bubbles in the ICM without producing noticeable observational features in the radio and X-ray band. However, for some clusters mass estimates have been derived from gravitational lensing. They were found to be in quite good agreement with mass estimates from X-ray observations suggesting that bubbles do not provide a significant fraction of

the pressure support in the cluster. Nevertheless, it is an important point that in clusters a lot of energy in the form of hot bubbles may remain unnoticed.

We computed the average displacement and dispersion of the ambient gas by the bubbles using tracer particles. The buoyant plasma was shown to be able to transport ambient gas to larger radii. Comparisons of the transport efficiencies of different runs suggests that, over a longer period, frequent low-power activity cycles are more efficient in stirring the environment than less frequent high-power outbursts of comparable energy output. Furthermore, we found that the transport is most efficient for gas near the injection point of the gas. Therefore, in a cooling flow cluster with a central galaxy, the most rapidly cooling gas is also most efficiently displaced.

It is difficult to estimate accurately what fraction of the energy of these subsonic motions will eventually be dissipated locally and what fraction will be carried (e.g. by sound waves and large scale motions) away from the cooling flow region. If the jet power is indeed $\sim 10^{44}$ erg/s then even a modest 10% efficiency of local dissipation into heat should be enough to exceed the radiative cooling of the gas.

However, we find that, with the given numerical scheme, it is difficult to estimate the dissipation reliably. The numerical diffusivity and viscosity impose uncertainties that are difficult to quantify exactly. We therefore urge great caution towards energy dissipation rates that are inferred from these kinds of simulations. In order to answer the important question of the energy dissipation into the ICM one needs simulations with a higher accuracy and higher resolution. This is work in progress and will be reported at a later time.

Some of the computations reported here were performed using the UK Astrophysical Fluids Facility (UKAFF). This work was supported by the European Community Research and Training Network ‘The Physics of the Intergalactic Medium’. MB also acknowledges support through a Junior Research Fellowship from Churchill College and thanks Jim Pringle for helpful discussions.

REFERENCES

- Baum, S. A. & O’Dea, C. P. 1991, MNRAS, 250, 737
- Berghöfer T.W., Bowyer S., Korpela E., 1999, in H. Böhringer, L. Feretti, and P. Schuecker (eds.), Diffuse thermal and relativistic plasma in galaxy clusters. MPE, p. 207
- Binney, J. 1999, Berlin Springer Verlag Lecture Notes in Physics, 530, 116
- Biretta, J. A. 1999, Berlin Springer Verlag Lecture Notes in Physics, 530, 159
- Böhringer, H., Voges, W., Fabian, A. C., Edge, A. C. and Neumann, D. M. 1993, MNRAS, 264, L25
- Böhringer, H., Nulsen, P. E. J., Braun, R. and Fabian, A. C. 1995, MNRAS, 274, L67
- Böhringer, H., 1999, Diffuse Thermal and Relativistic Plasma in Galaxy Clusters, eds. H.Böhringer, L.Feretti, P. Schuecker, MPE Report 271, 115
- Bolton J.G., Stanley G.J., Slee O.B., 1949, Nature, 164, 101
- Churazov, E. and Brüggen, M. and Kaiser, C. R. and Böhringer, H. and Forman, W. 2001, ApJ, 554, 261
- Churazov, E., Forman, W., Jones, C. and Böhringer, H. 2000, A&A, 356, 788
- Cowie, L. L., Hu, E. M., Jenkins, E. B. and York, D. G. 1983, ApJ, 272, 29
- David, L.P. et al., 2001, ApJ in press (astro-ph/0010224)
- Eilek, J. A., Melrose, D. B. and Walker, M. A. 1997, ApJ, 483, 282
- Eilek, J., Owen, F. and Zhou, F. 1999, Berlin Springer Verlag Lecture Notes in Physics, 530, 136
- Ekers, R. D. & Simkin, S. M. 1983, ApJ, 265, 85
- Enßlin, T. A. 1999, Diffuse Thermal and Relativistic Plasma in Galaxy Clusters, 275

- Fabian A.C., Sanders J.S., Ettori S., Taylor G.B., Allen S.W., Crawford C.S., Iwasawa K., Johnstone R.M., Ogle P.M., 2000, MNRAS, accepted, astro-ph/0007456
- Feigelson, E. D., Wood, P. A. D., Schreier, E. J., Harris, D. E. and Reid, M. J. 1987, ApJ, 312, 101
- Gull, S.F., Northover, K. J. E. 1973 Nature, 244, 80
- Harris D.E., Owen F.N., Biretta J.A., Junor W., 1999, Diffuse Thermal and Relativistic Plasma in Galaxy Clusters, eds. H.Böhringer, L.Feretti, P. Schuecker, MPE Report 271, 111
- Huang, Z. and Sarazin, C. L. 1998, ApJ, 496, 728
- Kaiser C.R., Dennett-Thorpe J., Alexander P., 1997, MNRAS 292, 723
- Kassim, N. E., Perley, R. A., Erickson, W. C. and Dwarakanath, K. S. 1993, AJ, 106, 2218
- Landau, L.D., Lifshitz, E.M., 1963, Fluid mechanics, Pergamon Press
- Leahy J.P., 1991, in P. A. Hughes (ed.), Beams and jets in astrophysics. Cambridge University Press, p. 100
- Loken, C., Burns, J. O., Norman, M. L., & Clarke, D. A. 1993, ApJ, 417, 515
- Loken, C., Roettiger, K., Burns, J. O., & Norman, M. 1995, ApJ, 445, 80
- Longair M.S., 1991, *High energy astrophysics*, Cambridge University Press
- Matsumoto, H., Koyama, K., Awaki, H., Tomida, H., Tsuru, T., Mushotzky, R. and Hatsukade, I. 1996, PASJ, 48, 201
- McNamara, B. R., O'Connell, R. W. and Sarazin, C. L. 1996, AJ, 112, 91
- McNamara, B. R., Wise, M., Nulsen, P. E. J., David, L. P., Sarazin, C. L., Bautz, M., Markovitch, M., Vikhlinin, A., Forman, W. R., Jones, C. and Harris, D. E. 2000, ApJ, 534, L135
- Mills B.Y., 1952, Nature, 170, 1063
- Norman, M.L., Smarr, L., Winkler, K.-H., Smith, M.D., 1982, A&A, 113, 285
- Nulsen, P. E. J. and Böhringer, H. 1995, MNRAS, 274, 1093
- Nulsen, P. E. J. 1986, MNRAS, 221, 377
- Nulsen, P. E. J. 1997, ASP Conf. Ser. 115: Galactic Cluster Cooling Flows, 135
- Onufriev, A.T. 1967, Zhurnal Prikladnoi Mekhaniki i Tehnicheskoi Fiziki, 2, 101
- Owen F.N., Eilek J.A., Kassim N.E., 1999, Diffuse Thermal and Relativistic Plasma in Galaxy Clusters, eds. H.Böhringer, L.Feretti, P. Schuecker, MPE Report 271, 107
- Owen F.N., Eilek J.A., Kassim N.E., 2000, ApJ: submitted, astro-ph/0006150
- Owen F.N., Eilek J.A., Keel W.C., 1990, ApJ 362, 449
- Owen, F. N. & Eilek, J. A. 1998, ApJ, 493, 73
- Peres, C. B., Fabian, A. C., Edge, A. C., Allen, S. W., Johnstone, R. M. and White, D. A. 1998, MNRAS, 298, 416
- Rizza, E., Loken, C., Bliton, M., Roettiger, K., Burns, J. O., & Owen, F. N. 2000, AJ, 119, 21
- Rottmann H., Mack K.-H., Klein U., Wielebinski R., 1996, A&A 309, L19
- Sarazin, C. L., Baum, S. A., & O'Dea, C. P. 1995, ApJ, 451, 125
- Saxton, C.J., Sutherland, R.S. & Bicknell, G.V., 2001, astro-ph/0107558
- Smith, M. D., Smarr, L., Norman, M. L., & Wilson, J. R. 1983, ApJ, 264, 432
- Soker, N. 1997, ApJ, 488, 572
- Soker, N. & Sarazin, C. L. 1988, ApJ, 327, 66
- Stone, J.M., Norman, M.L., 1992a, ApJS, 80, 753
- Stone, J.M., Norman, M.L., 1992b, ApJS, 80, 791
- Taylor, G. B., Perley, R. A., Inoue, M., Kato, T., Tabara, H., & Aizu, K. 1990, ApJ, 360, 41
- Tucker, W. and David, L. P. 1997, ApJ, 484, 602
- Walters, J.K. Davidson, J.F. 1963, J.Fluid.Mech., 17, 321

Zhao, J., Sumi, D. M., Burns, J. O., & Duric, N.
1993, ApJ, 416, 51

Zhidov, I.G. Meshkov, E.E. Popov,
V.V.Rogachev, V.G. Tolshmyakov A.I. 1977,
Zhurnal Prikladnoi Mekhaniki i Tehnicheskoi
Fisiki , 3, 75